D. R. Zimbelman · R. J. Watters · I. R. Firth ·
G. N. Breit · G. Carrasco-Nunez

Stratovolcano stability assessment methods and results from Citlaltépetl, Mexico

Abstract Citlaltépetl volcano is the easternmost strato-volcano in the Trans-Mexican Volcanic Belt. Situated within 110 km of Veracruz, it has experienced two major collapse events and, subsequent to its last collapse, rebuilt a massive, symmetrical summit cone. To enhance hazard mitigation efforts we assess the stability of Citlaltépetl's summit cone, the area thought most likely to fail during a potential massive collapse event. Through geologic mapping, alteration mineralogy, geotechnical studies, and stability modeling we provide important constraints on the likelihood, location, and size of a potential collapse event. The volcano's summit cone is young, highly fractured, and hydrothermally altered. Fractures are most abundant within 5–20-m wide zones defined by multiple parallel to subparallel fractures. Alteration is most pervasive within the fracture systems and includes acid sulfate, advanced argillic, argillic, and silicification ranks. Fractured and altered rocks both have significantly reduced rock strengths, representing likely bounding surfaces for future collapse events. The fracture systems and altered rock masses occur non-uniformly, as an orthogonal set with N–S and E–W trends. Because these surfaces occur non-uniformly, hazards associated with collapse are unevenly distributed about the volcano.

Depending on uncertainties in bounding surfaces, but constrained by detailed field studies, potential failure volumes are estimated to range between 0.04–0.5 km^3. Stability modeling was used to assess potential edifice failure events. Modeled failure of the outer portion of the cone initially occurs as an "intact block" bounded by steeply dipping joints and outwardly dipping flow contacts. As collapse progresses, more of the inner cone fails and the outer "intact" block transforms into a collection of smaller blocks. Eventually, a steep face develops in the uppermost and central portion of the cone. This modeled failure morphology mimics collapse amphitheaters present at many of the world's stratovolcanoes that have experienced massive failure events.

D. R. Zimbelman (✉)
G.O. Logic,
P.O. Box 1878, White Salmon, WA 98672, USA
e-mail: DZimbelman@gorge.net

R. J. Watters · I. R. Firth
Dept Geological Sciences MS 172,
University of Nevada,
Reno, NV 89557-0138, USA

G. N. Breit
DFC Bldg 20 MS 935, USGS Box 25046, Denver, CO 80225, USA

G. Carrasco-Nunez
Unidad de Investigacion en Ciencias de la Tierra,
Campus Juriquilla, UNAM,
Apdo. Postal 1–742, Qro. 76001 Centro Querétaro, Mexico

Introduction

Massive edifice failure events are common at many large andesitic stratovolcanoes (Siebert 1984). Failure volumes often exceed 1 km^3 and can lead to highly mobile and potentially devastating volcanic avalanches and debris flows (Hall and Mothes 1997). The avalanches high mobility has been attributed to magmatic-hydrothermal fluids and gases, pre-failure fracturing of the edifice, the presence of as little as 1–2% clays, and to the inclusion of water, which can be from the volcano itself or incorporated during transport from water-saturated sediments (Ui 1983; Voight et al. 1983; Costa 1984). Travel times for the avalanches have been estimated to be less than 12 min at distances of 20 km or more from their source (Voight et al. 1981). To assist with mitigation of hazards related to volcanic edifice failure we use a multidisciplinary approach to identify source areas and volumes for potential failure events at Citlaltépetl volcano, Mexico.

Very large volume failures ($n·10^9$ m^3), such as those from Citlaltépetl, Mount Rainier, and Mount Shasta

(Cascade Range, US), represent catastrophic, although infrequent hazards. At these volcanoes, the largest collapse events have included extensive amounts of hydrothermally altered rock (Crandell 1971, 1989; Carrasco-Nunez et al. 1993). Studies of several recently-exposed landslide surfaces have shown that they are commonly highly fractured and hydrothermally altered (Zimbelman 1996; Vallance 1999; van Wyk de Vries et al. 2000) and that the alteration can significantly weaken the volcanic rocks and precipitate edifice collapse and associated debris avalanches (Lopez and Williams 1993; Watters et al. 2000).

Stability of a volcanic cone is dependent on the strength of the volcanic materials, topography, and the influence of seismic forces and fluid pressure (Day 1996; Voight and Elsworth 1997). Of these factors, seismic forces and fluid pressures are generally studied after slope failure or volcanic activity, whereas rock strengths and stabilities can be calculated and evaluated prior to an event. For example, Reid et al. (2000), using data from Voight et al. (1983) and Watters and Delhaut (1995), concluded that the depth and volume of a failure mass is dependent on the rock strength. A key component in edifice stability, therefore, is the assessment of rock mass strength and its spatial distribution, including within the volcanoes interior. We tested rock strengths in the field and laboratory to zone the volcano's rock mass strengths. For the volcano's interior, rock mass strengths were established after we developed generalized geologic cross sections derived from our surface mapping results and by analogy with volcano-hosted mineral deposits. By determining a range of confined rock strengths that likely exist at depth, where potential failure surfaces may develop, we were able to evaluate the influence on slope stability of subsurface structures and altered or weakened rocks. Through a process of varying rock strength parameters, orientations and strengths along structures, and thickness' of lava flows and pyroclastic deposits, we quantitatively assess the volcano's slope stability and use the results to model potential failure events.

Geologic setting

Citlaltépetl (5,675 m), also known as Pico de Orizaba, is North America's highest volcano and third highest peak. Located within 100 km of the Caribbean coast, Citlaltépetl is the eastern most major volcano in the ca. 1,000 km Trans-Mexican Volcanic Belt (Fig. 1). According to Carrasco-Nunez (1997) and Carrasco-Nunez and Gomez-Tuena (1997), Citlaltépetl volcano consists of three superimposed stratovolcano cones, all of which were accompanied by dome intrusions. The cone-building events include, from oldest to youngest, the Torrecillas, Espolón de Oro, and Citlaltépetl stages (Fig. 2).

Citlaltépetl volcano, which most recently erupted in A.D. 1687 (Mooser et al. 1958), has produced two large-scale catastrophic edifice collapse events and associated hazards to nearby communities are considered substantial.

Subsequent to its two major collapse events, the edifice was reconstructed into one of the world's premier examples of a conical, glacially capped volcanic landform. Siebe et al. (1993) noted that the most important river basin originating on the volcano, the Rio Jamapa, contains no major cities or towns near the volcano; in contrast, the towns are located on topographic highs, areas that represent relative safety from collapse-related catastrophes that might have occurred in pre-Hispanic times and that could have induced the inhabitants to locate their towns to safer areas.

Pre-Citlaltépetl stages

The Torrecillas stage began about 500–650 ka and ended with an edifice collapse event at about 250 ka. This collapse partially removed the Torrecillas cone, forming a ca. 3.5-km crater, and produced the Jamapa avalanche, a voluminous (ca. 20 km^3) debris flow that traveled as far as 75 km to the Caribbean coast (Carrasco-Nunez and Gomez-Tuena 1997). Hubbard (2001) analyzed the pre-collapse Torrecillas edifice volume and alteration mineralogy, compared this with the Jamapa avalanche deposit volume and alteration mineralogy, and suggested that the former Torrecillas edifice was the source of the avalanche. Locally, uppermost outcrops of Torrecillas stage rocks are deeply eroded, heavily fractured, and altered to a maximum depth of about 200 m. Alteration minerals include ferric oxyhydroxides and various forms of silica, mostly as fracture coatings and network veinlets and, less commonly, jarosite and alunite group minerals, smectite, and, locally, kaolin.

Amphibole dacite eruptions at about 210 ka represent the initial phase of the second stage, the Espolón de Oro. This stage also terminated with edifice collapse, between 13 and 27 ka., resulting in the 1.8-km^3 Teteltzingo lahar. This clay-rich lahar, containing 10–16% smectite or kaolin, traveled 85 km and covered an area of 143 km^2 (Hoskuldsson and Robin 1993). Hubbard (2001) studied alteration mineralogy and a reconstructed edifice volume to assert that the former Espolón de Oro edifice was the likely source for the Teteltzingo lahar deposit. Locally, rocks from the Espolón de Oro stage are highly fractured and altered to argillic, silicic, and oxide assemblages in their upper parts, grading downward to less fractured and fresh units within 200 m. Alteration minerals include opal, cristobalite, hematite, goethite, alunite, jarosite, anhydrite, and kaolin.

Citlaltépetl stage

Citlaltépetl's symmetrical summit cone is the focus of this paper and was constructed during the volcano's third cone-building stage, after the two major collapse events. The summit cone includes historic lava flows, domes, block-and-ash flow deposits, and intensely fractured and hydrothermally altered rock masses (Carrasco-Nunez and
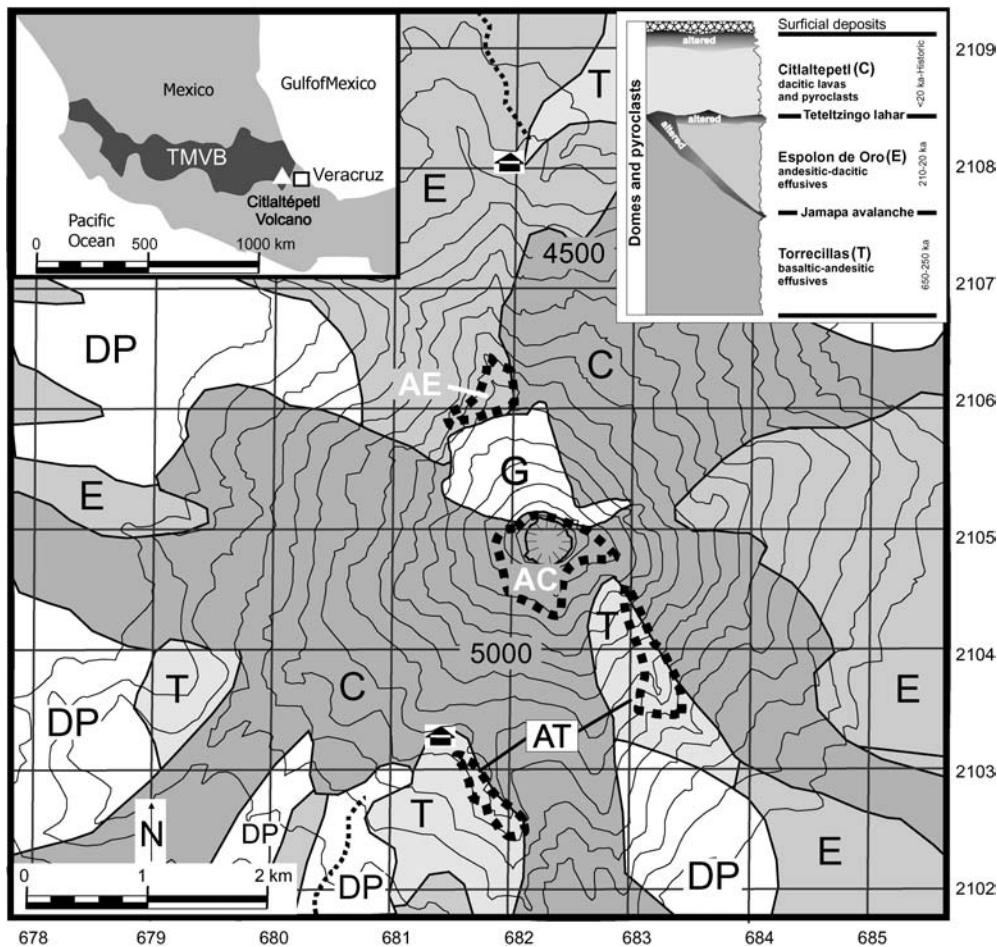
Fig. 1 Sketch map showing generalized geology and areas of hydrothermally altered rock above 4,100 m, Citlaltépetl volcano. Contours, 100 m, and 1-km UTM grid from the 1:50,000-scale Coscomatepec (E14B46; 1984) and Orizaba (I14B56; 1985) topographic maps. Geology generalized from Carrasco-Nunez and Ban (1994); *T* Torrecillas stage rocks and deposits; *E* Espolón de Oro stage rocks and deposits; *C* Citlaltépetl stage rocks and deposits; *DP* undifferentiated domes and pyroclastic flows and deposits; *G* glacier. *Heavy dashed lines*, hydrothermally altered outcrops: *AT* altered Torrecillas; *AE* altered Espolón de Oro; *AC* altered Citlaltépetl. *Hatched lines* Summit crater; *dotted lines* roads; buildings, south and north climber's huts. *Left insert* Index location map; *TMVB* Trans Mexico Volcano Belt; *triangle* Citlaltépetl volcano; *square* Veracruz. *Right insert* Generalized stratigraphic section showing major cone-building units, including altered rocks in their uppermost parts, and domes and pyroclasts throughout section

Gomez-Tuena 1997; Hubbard 2001). Partially covered by glacial ice, these rocks represent likely potential source materials for future collapse events. At Citlaltépetl, the Holocene has been dominated by at least five paroxysmal block-and-ash flow eruptions, each of which was followed by moderate ash and pumice falls, and andesitic lava flows from the summit crater (Cantagrel et al. 1984). The ash and scoria pyroclastic flows are predominantly dacitic or andesitic and were emplaced up to 30 km from the vent (Carrasco-Nunez and Rose 1995). Some of the flows underlie areas that are now heavily populated, including the city of Orizaba (pop. 180,000).

The crater interior consists of highly fractured layers of volcanic breccia, ash, scoria, and lava that host extensive zones of replacement alteration including massive, funnel-shaped zones and thinner selvage zones bordering fractures (Fig. 3). Alteration of the Citlaltépetl cone is on-going, with silicification and advanced-argillic alteration being developed adjacent to active fumaroles on the craters outer west rim (Fig. 4).

Methods

Fieldwork

Field-based geologic mapping was conducted during seven weeks spanning January 1999, January 2000, and March 2001. The mapping and mineralogic studies supplemented a remote-sensing study of the volcano (Hubbard 2001) and confirmed the presence of hydrothermally altered rock in all three cone-building stages. Rock samples were collected along ridges, within the crater and its rim, and across steep headwalls. Navigation was achieved with a hand-held GPS unit (ca. 30-m accuracy) using the Coscomatepec 1:50,000-scale topographic map as a base. The crater rim was mapped with a laser rangefinder (±1 m accuracy), compass, and clinometer (Fig. 5). Because the summit GPS measurements were
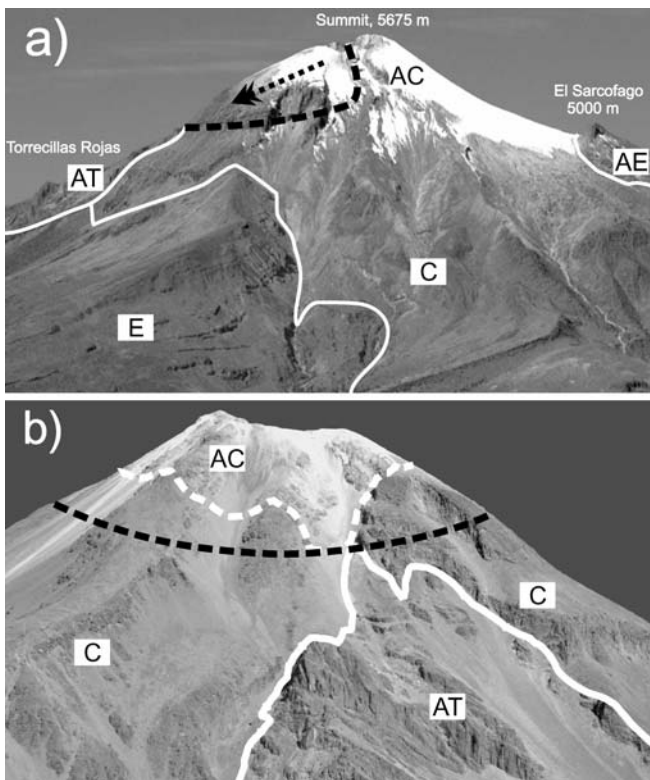
Fig. 2a, b East and south flanks, Citlaltépetl volcano showing modeled failure surface (*dashed black lines*) and failure direction (*arrow*), as discussed in text. **a** East flank; *AE* altered Espolón de Oro stage rocks; *AT* altered Torrecillas stage rocks; *E* unaltered Espolón de Oro stage rocks; *AC* altered Citlaltépetl stage rocks; *C* unaltered Citlaltépetl stage rocks. **b** South flank; contact between Torrecillas and Citlaltépetl stage rocks (*solid white line*) and contact between altered and unaltered Citlaltépetl stage rocks (*dashed white line*)
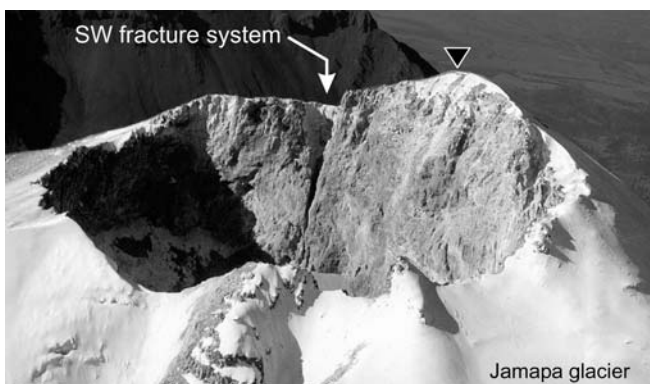
Fig. 3 Oblique aerial photo, looking southwest, into Citlaltépetl's summit crater and the SW fracture system; *triangle* summit; crater diameter ca. 400 m

made when selective availability techniques were used, horizontal position errors on the order of 100 m in the UTM positions are possible. Similar to most active stratovolcanoes, many areas on Citlaltépetl are mantled by snow, colluvium, talus, and young volcanic flows and deposits, rendering bedrock mapping difficult. These young surficial deposits can mask underlying structures and
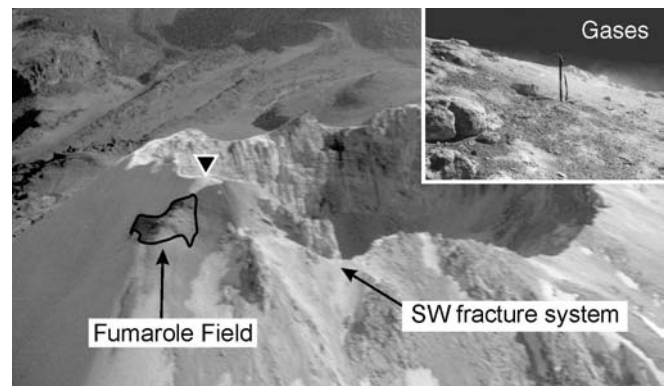
Fig. 4 January 2000, photograph of Citlaltépetl volcano's outer west crater rim showing active fumarole field; *triangle* summit. *Insert* Fumarole gases emanating through massive, clay-rich replacement; 70-cm axe for *scale*

alteration zones, making extrapolation of geology beneath the cover tentative.

Alteration mineralogy

Sixteen representative samples of hydrothermally altered rock were collected for mineralogy, petrology, and geochemical study from Citlaltépetl stage rocks (Fig. 5). The altered rocks include replacement and vein styles. For example, massive zones of kaolin and alunite replacement alteration were collected throughout the summit cone, and at the active fumarole field and vein alteration was collected where it was exposed, especially near the summit crater. Rock samples were studied by standard thin section, X-ray diffraction (XRD), and scanning electron microscopy (SEM). XRD analysis identified minerals present in bulk rock samples and mineral separates. Diffraction patterns were collected using copper K-alpha radiation on a Siemens D500 equipped with a graphite monochromator. Phase identification was facilitated using Jade 5.0. A JEOL 5800 scanning electron microscope equipped with an Oxford ISIS energy dispersive spectrometer system (EDS) was used to examine samples and acquire compositional data on fine-grained alteration phases.

Geotechnical studies

The geotechnical study concentrated on obtaining samples of the weakest rocks exposed on the Citlaltépetl cone and at the interface of the cone with older units. Generally, the samples were hydrothermally altered or closely fractured or sheared and from zones that represent major planes of weakness and could localize failure release surfaces. Edifice strength assessment consisted of a two-part field mapping program and followed procedures detailed in Watters et al. (2000). During the first part, rock structure information was obtained through systematic mapping of major shear or fault zones and collection of joint and bedding orientation and joint- and fracture-spacing data. The structural information was collected using a CLAR compass, an instrument developed explicitly for the rapid collection of rock discontinuities. Structural information was obtained to derive contoured stereoplots of joint sets and bedding attitudes. The second part included the collection of representative samples from which intact rock strengths, joint and infilling material strengths, and the type and intensity of alteration were evaluated. For the geotechnical component, hydrothermal alteration classification was based on visual observations, as described in Watters and Delhaut (1995), which varies from an intensity of zero (no alteration) to four (complete replacement of phenocrysts and matrix).

Fig. 5 Summit crater sketch, as mapped by laser binoculars, compass, and clinometer, with summary of alteration mineralogy as determined by XRD analyses; *boxes* approximate locations of fracture systems where they intersect crater rim; *dashed lines* fracture trends; *circles* sample sites; *light gray* crater interior; *dark gray* active fumarole field; *triangle* summit. UTM grid, 100 m. All samples contain various forms of silica, mostly cristobalite or opal, in addition to the minerals indicated. *alun* Alunite; *anhy* anhydrite; *gyps* gypsum; *kaol* kaolin; *mina* minamiite; *naalun* natroalunite; *sulf* sulfur; *yava* yavapiite
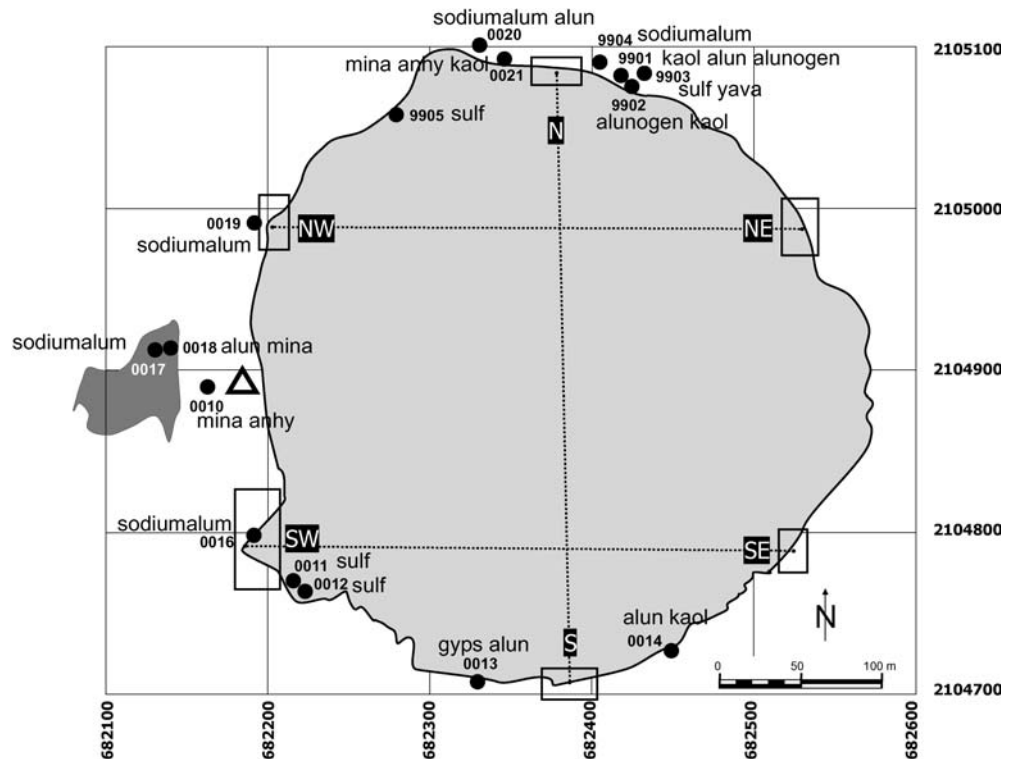
Stability modeling

Stability modeling studies are crucial to an accurate volcano stability assessment, as they show how changes in rock strength and/or internal geologic structure (bedding or shear zone orientations) can affect volcano slope stability. Models can be developed to assess which portions of a volcano will be the first to collapse, whether from gravity, seismic, or eruptive forces. If failure is very recent and can be monitored, as at Soufriére Hills volcano, Montserrat, sample collection and rock strength testing combined with slope modeling provide critical clues regarding the failure processes and the factors associated with collapse (Voight 2000).

Previous modeling studies have provided insight into volcano deformation and catastrophic collapse using two-dimensional limit equilibrium and numerical method techniques (Firth et al. 2000; Voight 2000). Three-dimensional limit equilibrium methods were used by Reid et al. (2000) to study the 1980 Mount St. Helens collapse where topographic effects could be incorporated into the analysis. The limit equilibrium method does not provide displacement information throughout the slope, but yields a factor of safety for the slope by obtaining the critical slip surface. Numerical modeling is useful to evaluate slope movements at different depths below a volcanoes surface and provides observations of failure processes through input of different rock strengths and/or structures into the model and proved more useful at Citlaltépetl.

Firth et al. (2000) applied a distinct element modeling (UDEC) numerical method to investigate the sequential and retrogressive nature of stratovolcano slope failures. In this method, a rock mass is represented as an assemblage of discrete blocks. The contact forces and displacements at the interfaces of a stressed group of blocks are established through a series of calculations that trace the block displacements. During this dynamic process, the propagation rate is a function of the physical properties of the discrete system. The boundaries between individual blocks or groups of blocks can be assigned different strength characteristics to reflect changes from chemical alteration, faulting, or lithologic variations. Using the time stepping function of UDEC, the model can be allowed to fail and the velocity and displacement history of specific blocks traced. The influence of varying physical and mechanical properties within
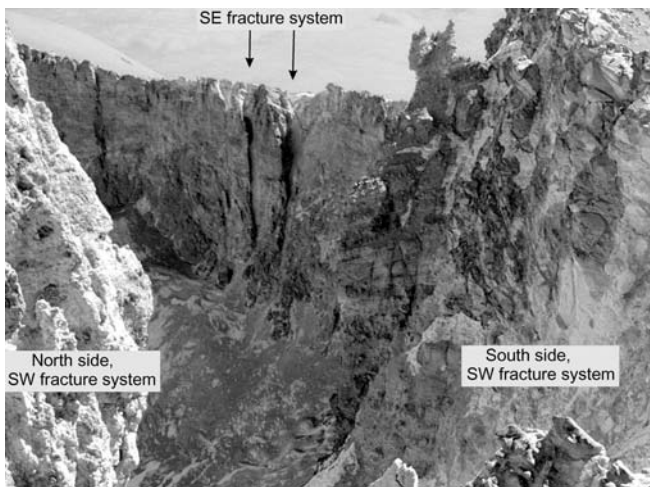
ranges obtained from field and laboratory strength tests can be investigated with or without a collapse event. The analysis is valid for a variety of slope failures including relatively frequent, smaller failures and less frequent, massive failures. Additionally, UDEC provides accurate velocity and volume information that can be incorporated into run-out models for use in hazard assessments.

Results

Field studies

The Citlaltépetl cone contains bedded volcanic units with an average dip of about 35°, which is steeper than the 20 to 30° dips of the underlying Espolón de Oro or Torrecillas rocks. At its summit, the cone includes active alteration related to fumaroles on the craters west flank and extensive areas of altered rock exposed on the cones outer flanks and within its summit crater walls. The fumarolic gases emanate from an irregularly shaped field about 50 m west of the summit, which apparently fluctuates in size. In January 2000, the zone of fumaroles occupied about 2,000 m² whereas, in March 2001, the fumarolic area emitted gases more vigorously and occupied a larger area, approximately 6,000 m². The fumarolic gases emanate through cream, gray, and orange silicified or clayey zones surrounding scattered corestones within matrix-supported volcanic breccia, through fractures in the breccia, and through a silicified hard-pan surface that locally reaches a thickness of 30 cm (Fig. 4).

The summit contains a ca. 400-m diameter, approximately circular crater rim that dips to the east at about 23° and is cut by numerous fractures (Fig. 3). Exposed along

Fig. 7 Pervasive replacement (PR) of porphyritic volcanic flow rock by very-fine-grained alunite and kaolin coated by native sulfur veinlet (sulfur); field of view 35 cm

Fig. 6 Eastward view of SE and SW fracture systems, Citlaltépetl's summit crater. Foreground, north (*left*) and south (*right*) sides of SW fracture system; note intense fracturing and alteration of host volcanic rocks. Background, *arrows*, SE fracture system. Field of view, ca. 50 m. See Fig. 3 for southwestward view of SW fracture system

the crater rim are six large, high-angle fracture clusters and many smaller fractures and fissures (Fig. 5). The six main fracture clusters intersect the crater rim along its N, S, NE, NW, SE, and SW sectors. These fractures define two main fracture orientations within the summit cone, trending 092 (EW) and 358 (NS). Generally, within a zone of 5 to 20 m, both the N–S and E–W fracture systems intersect the crater rim as five or more subparallel fractures spaced about 0.5 to 2 m apart (Fig. 6) and include fissures as wide as 15 m (SW fracture system; Figs. 3 and 6). Where Citlaltépetl rocks are exposed and accessible, including the summit crater and the south, west, and east portions of the cone, many of these fracture systems and bedding surfaces are highly altered, with their surfaces coated with kaolin and/or sulfates.

Alteration mineralogy

Altered rocks occur throughout the summit, mostly as pervasive to selective replacement by acid sulfate, advanced argillic, argillic, and silicified ranks and as local surface precipitates and fracture fillings of native sulfur, gypsum, anhydrite, and other sulfate minerals (Fig. 7). As exposed along the interior crater walls, some of the alteration reflects the surface manifestation of upward-flaring replacement pipes (Fig. 8). Within the pipes, alteration occurs as intensive acid-sulfate minerals pervasively replacing and cross cutting various volcanic host units, including massive lava flows.

Altered rocks consist of various forms of silica, mostly opal and cristobalite, kaolin, and sulfur-bearing minerals that can be classified into five groups: (1) alunite $(KAl_3(SO_4)_2(OH)_6)$ and its chemical analogs such as natroalunite $(NaAl_3(SO_4)_2(OH)_6)$ and minamiite [(Na,Ca,-
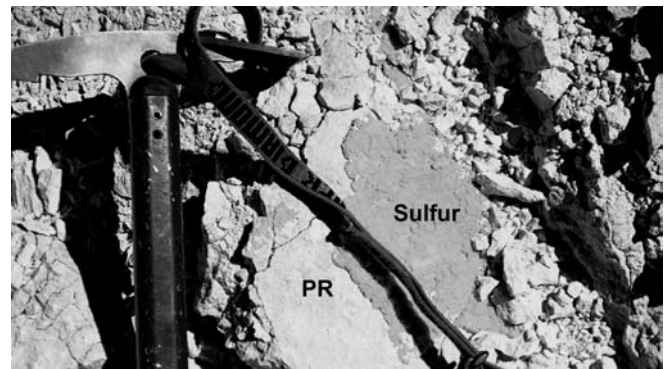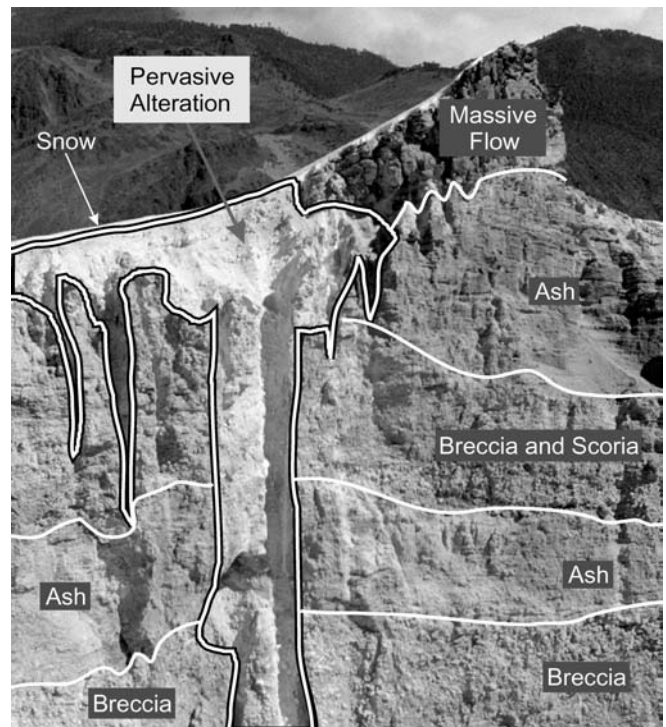
Fig. 8 North fracture system with upward-flaring zone of massive, hydrothermally altered rock, north interior wall, Citlaltépetl's summit crater

K)$Al_3(SO_4)_2(OH)_6$]; (2) jarosite [$KFe_3(SO_4)_2(OH)_6$]; (3) soluble Al-hydroxy sulfate, including alunogen [$Al_2(SO_4)_3$ $17H_2O$], meta-alunogen]$Al_2(SO_4)_3$ $12H_2O$], and sodium alum [$NaAl(SO_4)_2$ $12H_2O$]; (4) simple sulfates such as gypsum ($CaSO_4$ $2H_2O$), anhydrite ($CaSO_4$), yavapiite $KFe(SO_4)_2$, and barite ($BaSO_4$); and (5) native sulfur (S; Table 1). Results from the XRD analyses indicated a range in sulfate mineral phase compositions, particularly in alunite-group minerals. The XRD peak shapes and positions were consistent with the presence of alunite, natroalunite, and minamiite as well as phosphate analogs. Scanning electron microscope

Table 1 XRD results, Cit-laltépetl stage hydrothermally altered rocks. Alteration intensity after Watters and Delhaut (1995)

| Sample	XRD alteration mineralogy	Alteration rank, style, intensity
9901	Kaolin, alunite, cristobalite, opal, alunogen	Acid-sulfate, replacement, 4
9902	Alunogen, kaolin, meta-alunogen, tridymite	Advanced argillic, replacement, 4
9903	Sulfur, yavapiite, opal, cristobalite	Silicification, replacement and veining, 4
9904	sodium alum opal cristobalite	Advanced argillic, replacement, 3–4
9905	Sulfur, opal, cristobalite	Silicification, replacement and veining, 3
0010	Cristobalite, minamiite, anhydrite	Advanced argillic, replacement, 3
0011	Cristobalite, opal, sulfur	Silicification, replacement and veining, 3–4
0012	Cristobalite, opal, sulfur	Silicification, replacement and veining. 3–4
0013	Cristobalite, opal, gypsum, alunite	Acid-sulfate, replacement and veining, 4
0014	Opal, tridymite, alunite, kaolin	Acid-sulfate, replacement, 3
0016	Cristobalite, tridymite, sodium alum	Advanced argillic, replacement, 3–4
0017	Cristobalite, minamiite, alunite	Acid-sulfate, replacement, 3–4
0018	Cristobalite, tridymite, sodium alum	Advanced argillic, replacement, 3
0019	Cristobalite. tridymite, sodium alum	Advanced argillic, replacement, 4
0020	Cristobalite, tridymite, opal, sodium alum, alunite	Acid-sulfate, replacement, 4
0021	Cristobalite, minamiite, anhydrite, kaolin	Advanced argillic, replacement, 4
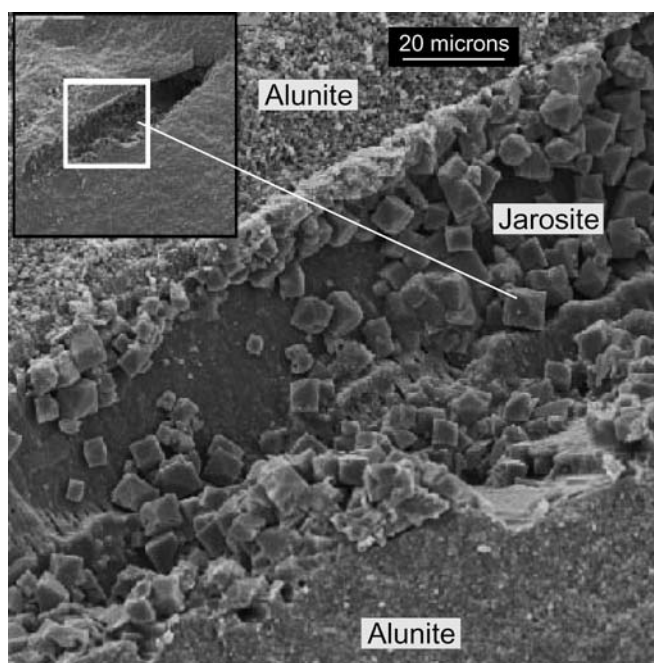
Fig. 9 SEM micrograph of jarosite crystals in a prismatic cavity surrounded by alunite

study of sulfur-bearing phases determined that most are fine grained and have complex spatial associations and results of the SEM-EDS confirmed the compositional variation of alunite phases indicated by the XRD data. Alunite generally occur as 1-μm or smaller cubes, with some crystals having lengths to 10 μm and jarosite occurs within cavities, as micron-sized crystals, surrounded by more massive but finer-grained alunite (Fig. 9). Native sulfur, gypsum, anhydrite, and barite occur as millimeter- to centimeter-scale vein fillings or fracture coatings (Fig. 10).

Zimbelman et al. (2003) determined stable isotope data for altered rocks from five active stratovolcanoes, including Citlaltépetl. Stable isotope data help to define the processes that produce aqueous sulfate in different environments during stratovolcano evolution. Understanding these processes is key to interpreting the extent of alteration and, thus, the extent of potentially weakened rock within the volcanic edifice's interior. Zimbelman et al. (2003) summarized the stable isotope signatures at Citlaltépetl as follows: alunite minerals have δD and $\delta^{18}O_{SO4}$ values that indicate an important role of magmatic fluids in their origin; jarosite minerals have $\delta^{18}O_{SO4}$ values that indicate meteoric water was important

Fig. 10 SEM backscatter images of barite and silica
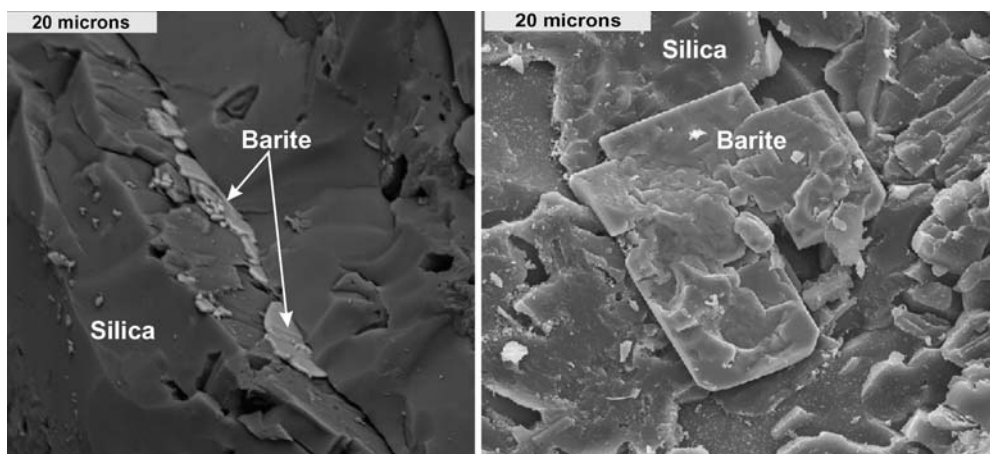
during their evolution; barite minerals have $\delta^{34}S$ and $\delta^{18}O$ values consistent with an origin from magmatic brines that mixed with meteoric water containing sulfate derived from the oxidation of H_2S or pyrite; native sulfur is derived from the oxidation of H_2S; and soluble Al-hydroxy sulfates formed after repeated cycles of condensation and evaporation associated with acid solutions.

Geotechnical studies

Fracture orientation data for 53 structural measurements from the Citlaltépetl cone are presented in Fig. 11. This stereogram illustrates that the fracture distribution is not random, but has dominant orientations that effectively divide the cone into distinct blocks. At the summit, the predominant structural feature is an E–W-striking shear zone, possibly a fault, while three dominant joint sets characterize the cone, with a girdle of poles representing bedding flows (Fig. 11). Two joint sets strike approximately N–S, with steep dips of about 70°E and 70°W. A third set strikes approximately E–W, corresponding to the observed shear zone cutting the summit, and also dips steeply, at 70°S. Most of the fractures, joint sets, and bedding surfaces contain veneers or infillings of hydrothermally altered material.

The field and laboratory rock strengths were derived from intact samples collected at the same sites where joint and bedding orientations were measured in the field and are summarized in Tables 2 and 3. The strength results are presented as the unconfined compressive strength, cohesion, friction, and shear stiffness. The unconfined strength represents the overall rock strength and consists of the cohesion and frictional strength. The cohesion and frictional strength characteristics are used in slope stability analysis and, when combined with the shear stiffness, allow for numerical modeling. Shear strength and stiffness results vary as a function of alteration intensity and density (Table 3). In general, hydrothermal alteration, other than silicification, produces a lower density rock with a corresponding reduction in strength,
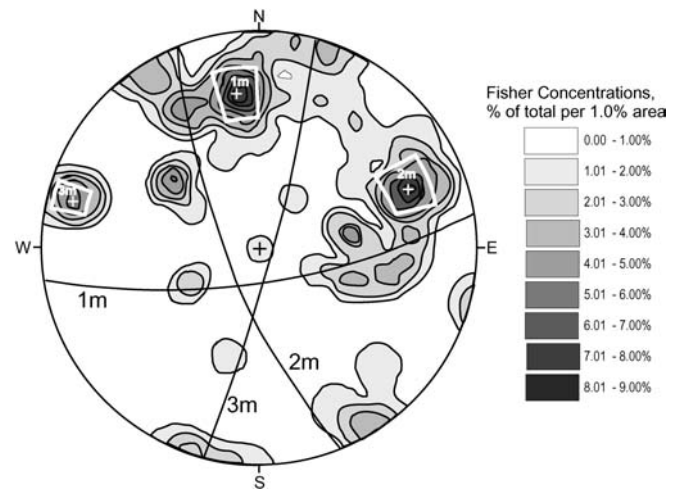
Fig. 11 Contoured stereogram from 53 joint and bedding surface measurements, Citlaltépetl cone. Three major joint concentrations occur, labeled *1 m*, *2 m*, and *3 m*. Great circles are plotted for each of the three concentrations and correspond to east–west and north–south joint sets

as illustrated by the unconfined compressive strength results (Table 2). The shear strength testing of joints and bedding surfaces established an envelope of values of normal and shear strength and stiffness for joint and bedding surfaces within the cone, and reflects different alteration intensities (Table 3). Increased alteration intensities correspond to lower strengths and measured and calculated rock strength friction and cohesion values show that the lowest strengths are in altered rocks and along altered joints and bedding surfaces. Rock strengths for Torrecillas and Espolón de Oro stages beneath the Citlaltépetl cone are generally stronger (less altered) than those for the overlying Citlaltépetl cone (Table 4). The strength results show that an anisotropic rock mass strength exists in the volcanic edifice, with sectors of the summit consisting of massive, weak rock bounded by highly altered and weakened steep to vertical fracture systems, and variably altered, outward-dipping flows.

Table 2 Summary of unconfined compressive strength for fresh and altered volcanic rocks. Alteration intensity after Watters and Delhaut (1995)

| Alteration intensity	Rock density (g/cm^3)	Average strength (MPa)	Standard deviation (MPa)	Strength range (MPa)	Number of tests
0	2.5	146	43.4	196–120	15
2–4	1.7–0.8	34.7	17.4	57.8–8.6	32

Table 3 Summary of shear strength and stiffness data from shear zones, joints, and bedding surfaces. Alteration intensity after Watters and Delhaut (1995)

Alteration intensity	Alteration type	Rock density of surface (g/cm^3)	Friction degrees	Cohesion (MPa)	Shear stiffness (MPa/mx10^3)
0	Unaltered	2.5	34	0.96	17.93
1–2	Acid sulfate	2.4	39	0.21	2.76
3–4	Acid sulfate	1.04	24	0.07	0.49

Table 4 Summary of laboratory testing results for unconfined compressive strength and shear strength for Espolón de Oro and Torrecillas stages rocks

Stage	Rock density (g/cm³)	Average strength (MPa)	Standard deviation (MPa)	Friction degrees	Cohesion (MPa)
Espolón de Oro	2.3–2.55	120	65	30–34	0.21–0.45
Torrecillas	2.3–2.6	183	58	33–39	0.45–0.7

Fig. 12 East–west cross section through Citlaltépetl volcano schematically representing the three-dimensional extent of alteration. *A* Altered core; *AO* altered pre-Citlaltépetl stage rocks; *C* Citlaltépetl stage rocks; *O* pre-Citlaltépetl stage rocks; *I* hydrovolcanic plumes associated with degassing magmas
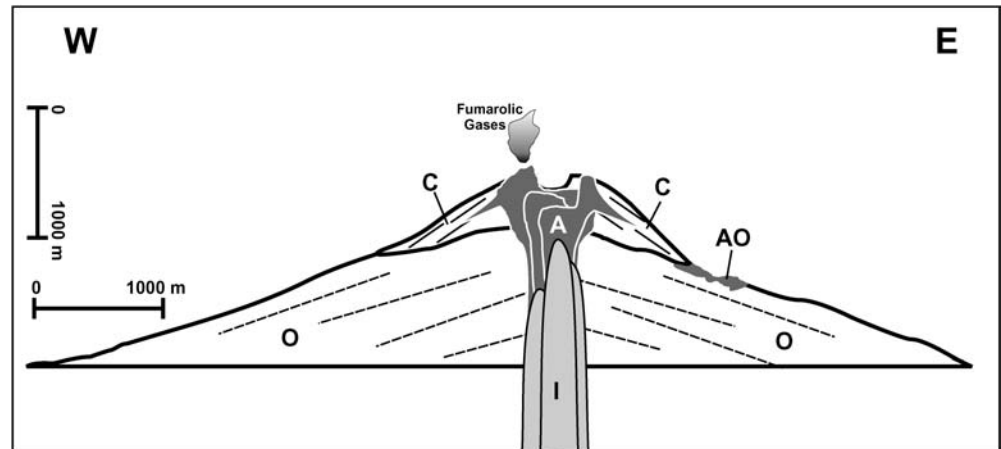

Geologic cross sections

After the mapping, mineralogy, geochemical, and structural data were collected it was possible to use the results to construct cross-sectional diagrams of the volcano's interior. Because many volcanic-hosted mineral deposits have three-dimensional information as a result of mining or drilling, they provide abundant information on the spatial distribution of alteration and fractures in similar environments to Citlaltépetl volcano. In a general sense, but based on hundreds of specific examples, volcanic-hydrothermal systems consist of buried, central intrusive bodies with overlying and, in places, overlapping alteration envelopes (Henley and Ellis 1983; Sillitoe and Bonham 1984; Sillitoe 1989, 1994; Hedenquist et al. 1996). As the buried intrusives cool, exsolved fluids will vertically rise towards the surface, generating hydrothermally altered rocks. In these systems, a complex series of processes occur, including fluid condensation, mixing, boiling, neutralization, and others, the net result of which are zones of acid-leached, hydrothermally altered, and structurally weakened volcanic host rocks above the buried intrusive sources. Our results are compatible with Citlaltépetl's altered rocks representing the uppermost part of a vertically extensive environment that was episodically developed above high-level, buried magmas that drove volcanic-hydrothermal systems.

For our purposes, cross-sectional geological models of the volcano's interior were kept simple, in part because without drill data this is a necessity, but also to allow us to input readily identifiable and essential features into the stability modeling program. Below about 5,000 m elevation, the cross sections consist of older, pre-Citlaltépetl stage volcanic rocks that generally dip at 25° or less with scattered, isolated altered outcrops that have less than 200 m in vertical extent (Fig. 12). We believe that the lack of extensive alteration and the low-angle of these volcanic units both represent the fact that these lower volcanic units are remnants of older (pre-Citlaltépetl stage) cones, the top (and more altered) parts of which were removed during catastrophic collapse events. Overlying the older units is the young Citlaltépetl-stage cone, with primary volcanic rock dips that average about 35°. Heavily altered and fractured throughout, but particularly in its central 500–700-m core, the cone also hosts ongoing fumarolic activity. The presence of abundant replacement acid sulfate and advanced argillic alteration assemblages at Citlaltépetl's summit, and through an exposed vertical extent of more than 675 m on its outer slopes, is compatible with alteration extending into the volcano's interior, at least to the base of the Citlaltépetl cone.

Stability modeling

After the geologic cross sections were constructed it was possible, by modeling, to quantify the strength for individual sectors, bounded by particular joint sets, bedding planes, and/or shear zones. UDEC models were used to analyze how possible failure scenarios would be controlled by the interplay of geologic structures and rock strengths. The UDEC models required the input of internal geologic structural information including joint and bedding orientations, strength data, rock densities,
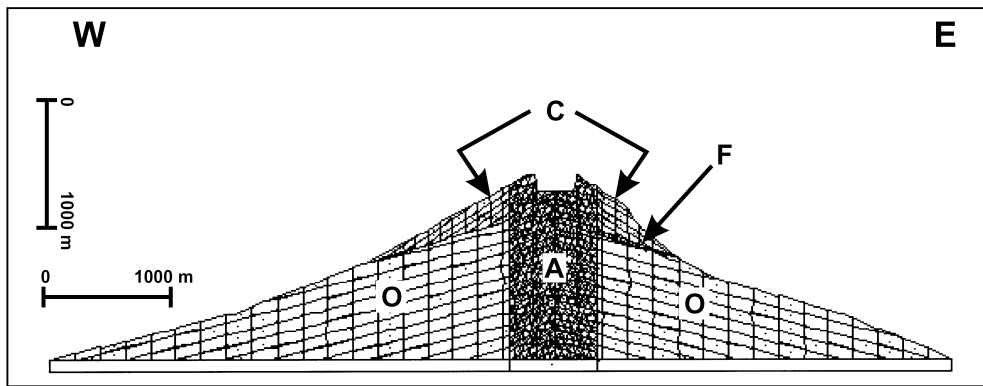
Fig. 13 East–west structural model of Citlaltépetl cone with north–south joint sets that dip 70° to the west and east, and bedding dips of 35° in the Citlaltépetl cone and 25° in underlying rocks; *A* altered core; *C* Citlaltépetl stage rocks; *O* pre-Citlaltépetl stage rocks; *F* closely-spaced fracture set, east side contact between Citlaltépetl stage and older stage rocks

Table 5 Strength data used for modeling studies

| Area	Rock density (g/cm³)	Friction degrees	Cohesion (MPa)	Shear stiffness (MPa/mx10³)
Core	1.6	10	0.07	100
Citlaltépetl Cone	2.5	20	0.14	100
Contact	1.6–2.0	10–15	0.07–0.10	100
Espolón de Oro Cone	2.5	30	0.45	1,000

and topography, although certain simplifying assumptions were necessary.

The basic structural grid model developed for the UDEC analysis is shown in Fig. 13 and is based on the joint and bedding orientations presented in Fig. 11, on data obtained during field mapping, and on simplified geology derived from the geologic cross sections. Geologically, the model contains three different rock masses including an altered core, an upper and young (Citlaltépetl) cone, and the older and underlying volcanic domes and cones. Structurally, models that use the actual joint separation distances are not possible as the computing time is prohibitive, so distances between joints and bedding surfaces were increased to overcome this limitation, without a loss in displacement characterization. In the model, the rock underlying the Citlaltépetl cone has joint and bedding surface distances between 100 and 200 m. For the Citlaltépetl cone, distances were fixed at 50 m, which allowed us to clearly observe the block interactions and slope movements. Failures were induced with block sizes (bed and joint separation distance) ranging from 10 to 100 m, with most analyses having 25- to 50-m spacings. A closely jointed zone was incorporated into the model for the east facing slope at the contact between the new and old cones, which reflects the low strength altered rock in this area.

A range of different rock shear strengths was assigned to the core, joints, and bedding planes, and cross sections of various orientations were analyzed. If the higher rock strengths in Table 2 were used, i.e., larger cohesion and friction values, the slopes remained stable, even when using the steepest topographic profiles from the south-eastern portion of the cone. Failure could only be developed when bedding dips were increased to more than 50°, which is too steep to be realistic. In contrast, keeping the internal structure consistent with the field mapping results (20–35° slopes) and lowering the rock strengths to correspond to 3–4 alteration intensity levels resulted in modeled slope failures (Table 5). Failures were not uniform, consistently occurring in only the ESE sector. Rocks in this sector have the steepest slopes and contain significant amounts of altered materials in their outwardly dipping beds. Thus, excluding seismic forces and fluid pressures that can precede or develop during an eruption, cone instability at Citlaltépetl volcano depends on intensity 3–4 alteration existing on critically oriented bedding planes and surfaces within the edifice. For modeled failure to occur, the volume of alteration is not critical; rather it is the presence of highly altered material on critical bedding planes, joints, or other surfaces within the edifice.

The influence on failure mechanisms of using only one or both of the two N–S fracture systems was also investigated. Initially, we modeled stability with only the west-dipping N–S joint set (Fig. 14). Selecting a low alteration strength for jointing and bedding and the lowest strength for the core, the rock mass surrounding the crater core displaced in an easterly direction as an "intact block". During the first 10 s, failure occurred along bedding and joint surfaces, but after about 10 s, support to the core was removed and an initial toppling failure mode resulted (Fig. 14a). Further displacement, at 20 s, caused the "intact block" to begin to break up and continued displacement transformed the toppling "intact block" into
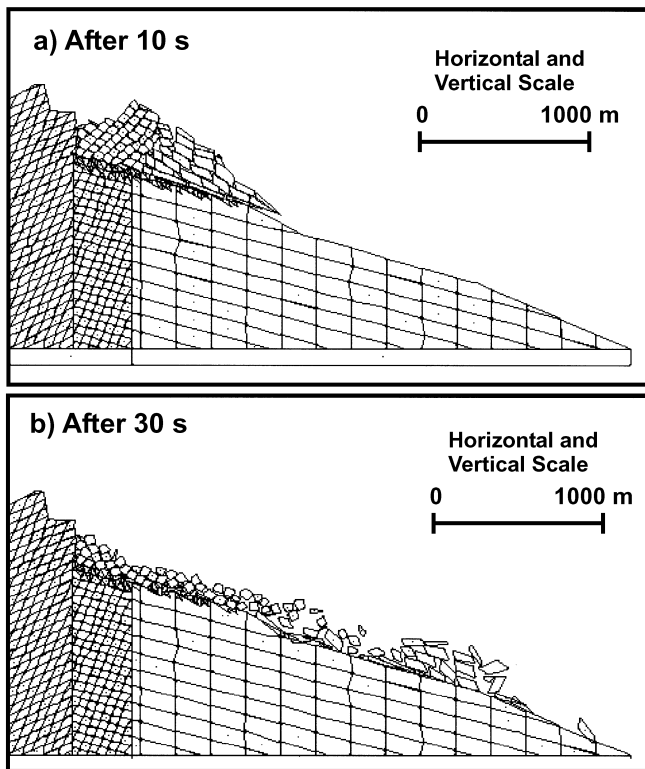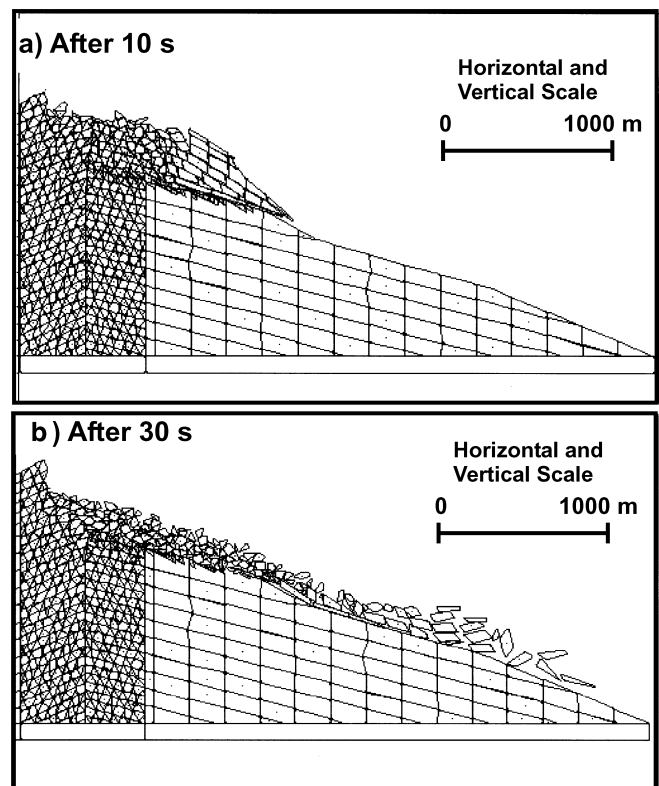
Fig. 14 Failure mode of cone with one joint set. **a** At 10 s after failure initiation, outer mass topples as an "intact block"; **b** at 30 s after failure initiation, "intact block" breaking into smaller blocks

Fig. 15a, b Failure model of cone with two joint sets. **a** At 10 s after failure initiation., "intact block" develops but toppling failure does not occur because of block failure along the steeply dipping easterly joint set; **b** at 30 s after failure initiation, "intact block" has begun to break into smaller blocks and the characteristic collapse amphitheater morphology evolves

a chaotic mass of individual blocks some 30–40 s after the initial failure (Fig. 14b).

Constructing a model with both sets of N–S joints, one set steeply dipping to the east and the other to the west, resulted in the outer mass failing as before as an "intact block". However, in this scenario, the core no longer failed in a toppling mode, as the steeply dipping easterly joint set promotes smaller-scale failures (Fig. 15). Models using both joint sets produced a morphology that resembles summit amphitheaters at many active strato-volcanoes, with the summit containing a steep headwall (Fig. 15b). The modeled headwall is somewhat ragged in section, reflecting the large block sizes we used. A smaller block size would produce a smother profile comparable to many actual failure headwalls.

Discussion

As noted by Siebert (1984) and Siebert et al. (1987), large-scale volcanic edifice collapse can be categorized as Bezymianny-type where associated with magmatic components or as Bandai-type where associated with phreatic activity. Because it is likely that a magmatic eruptive event would be preceded by significant seismicity and could be predicted, we have focused on the stability and potential edifice failure events that may not be preceded by significant precursory signals.

Citlaltépetl volcano is important because it represents potential hazards to more than 1 million people. Relative to many of the world's other large stratovolcanoes, Citlaltépetl has a simple collapse history, producing only two major collapse events. In some ways this makes it easier to study; on the other hand, it also implies that if the volcano does collapse again, the event may be very large, with the potential for far-reaching devastation. Most, if not all, of the geologic elements considered essential to large-scale collapse are present at the volcano. These include a large and voluminous edifice at great height relative to its surroundings, and its associated potential energy; hydrothermally altered rock zones, along which the edifice is structurally weakened; and major discontinuities, including highly-fractured rock masses and high-angle, open-space fractures.

Both the style and distribution of hydrothermally altered rock at Citlaltépetl volcano affect edifice stability. In the oldest, Torrecillas-stage alteration consists of silicified and oxidized volcanic rocks with similar or increased strengths relative to unaltered rocks. The middle stage rocks (Espolón de Oro) contain argillic, silicic, and oxide altered zones, but only locally, through a vertical extent of 200 m, mostly in the Sarcofago Peak area. The exposed outcrops of Torrecillas- and Espolón de

Oro-altered rocks suggest that most of their previous (overlying) altered rocks have been removed during the volcano's two major collapse events. What remains of these two stages is either unaltered, in the lowermost flanks of the volcano, or altered but are relatively strong rock masses in their uppermost outcrops, near 5,000 m elevation. In contrast, alteration in the Citlaltépetl-stage rocks is widespread and important because it has produced reduced rock strengths and because it occurs in the uppermost parts of the volcano, where potential energy is at a maximum.

Altered rocks exposed in the Citlaltépetl cone occur throughout much of the upper 675 m of the volcano and are localized by numerous fractures (Figs. 5 and 8). The alteration includes massive zones of replacement alteration and vein selvages and fillings along numerous fractures. Much of the replacement alteration is of acid sulfate or advanced argillic ranks, which is important from a stability perspective because it implies that acidic fluids have circulated through the volcano's interior. During vapor condensation, the SO_2 responsible for the alteration will be disproportionate and a fluid of very low pH can form. This acid fluid reacts with the host rocks, creating what Rye (1993) termed a "chimney of permeability". Because much of the Citlaltépetl-stage cone includes acid sulfate and advanced argillic alteration, it suggests that acid leaching and reduced strength rocks also occur within the volcanoes central conduit, beneath the summit crater, probably to a depth of at least 5,000 m elevation.

The configuration of open-space fractures suggests that the uppermost crater rocks may have slumped into the central conduits throat, and the upward-flared zones of pervasive alteration (Fig. 8) also demonstrate high permeabilities associated with the central conduit beneath the crater. For these reasons, we believe that the most likely "head" scarp surface for a future failure of the summit cone would approximately follow the trend defined by the E–W (Figs 3 and 6) fractures exposed on the crater rim. The lower failure surface would likely be above the relatively strong Torrecillas- and Espolón de Oro-stage rocks, near the 5,000-m elevation level. Depending on uncertainties in the various boundaries, failure volumes range from 0.04–0.5 km^3. Figure 2 shows part of this mass of Citlaltépetl-stage rock that is considered most likely to fail in a future, massive edifice collapse event. The modeling studies indicate that if rocks in these configurations have strengths that reflect alteration intensities of 3–4, failure could occur. However, because the Citlaltépetl cone has not failed, higher rock strengths must exist along the boundaries reflecting either the presence of less altered material along these surfaces, flatter lying boundaries, or other controls. Geotechnical data and modeling results suggest that failure of the cone without significant transient forces will not occur unless lower strength, hydrothermally altered rocks are developed. At Citlaltépetl, the stability analyses demonstrate that the central core of the volcano, comprised of the weakest and most altered rock, is buttressed by the outer,

less altered and stronger parts of the cone. Instability can be induced by supplementary alteration of the core or outward-dipping units.

The geotechnical and modeling results suggest that rock strength zonation and slope stability modeling could be combined with crustal ground deformation studies to analyze regions of potential sector failure at other active volcanoes. The relevance of geologic mapping to volcano deformation studies was highlighted by Amelung et al. (2000), who observed that uplift calculated from interferometry (InSAR) measurements is affected by existing fracture and fault orientations on a volcanic edifice. The largest movements were related to existing faults and ground fractures. Similarly, ground deformations were found to be highly variable as a result of fracture systems previously mapped on the south side of Sierra Negra volcano, Galapagos (Reynolds et al. 1995). Thus, a combination of results from methods such as those we present here and from remotely-sensed methods may prove valuable to aid in hazards mitigation efforts. This may be especially true for logistically difficult sites or when results are needed in short time periods, such as during periods of volcanic unrest.

Conclusions

Citlaltépetl volcano has experienced three main cone-building stages and two massive failure events. Erosion surfaces from the previous failures are well exposed and represent likely bounding planes for future edifice collapse events. High-angled fractures are locally concentrated, producing strikingly reduced rock strengths, especially within N–S- and E–W-trending systems. Similarly, areas of hydrothermally altered rock are locally important and, in places, have significantly reduced rock strengths. The alteration is most intensive within the major fracture systems, where it obtains acid sulfate and advanced argillic ranks and probably occurs beneath the summit crater through a depth of more than 675 m.

Detailed geologic mapping, mineralogy, and geotechnical studies reveal non-uniform distributions of structures and altered rocks and allow for realistic constraints to be input into a stability model. Depending on uncertainties in bounding surfaces, but constrained by the field and laboratory studies, failure volumes range between 0.04–0.5 km^3. Stability modeling of this mass was used to assess potential edifice failure events. The outer part of the cone initially fails as an "intact block" and, as the failure progresses, more of the inner core fails and the outer "intact" block transforms into a collection of smaller blocks, with increasing velocities. Eventually, a distinct morphology that includes a steep headwall is produced where the uppermost portion of the core existed. This modeled failure morphology mimics amphitheater failure surfaces present where collapse is known to have occurred at other stratovolcanoes.

Stability modeling studies can be used to accurately assess the non-uniform distribution of potential edifice

failure masses at many active volcanoes. However, logistical and fiscal realities probably dictate that such studies won't be conducted at many of the world's large stratovolcanoes, even when justified from a risk mitigation perspective. A possible solution is to apply the information on structures, alteration, and rock strengths we present here and use it in conjunction with remote-sensing methods. Such a combined approach could lead to more accurate assessments of volcanic hazards and, in emergency situations such as when a volcanoes activity level is changing suddenly, could be completed within short time frames. While we recognize that no one can accurately assess a future volcanic edifice failure, we believe that the methods we've developed present an important contribution towards quantitatively assessing the non-uniform geologic characteristics that control stability at most large volcanoes.

References

Amelung F, Jonsson S, Zebker H, Segall P (2000) Widespread uplift and "trapdoor" faulting on Galapagos volcanoes observed with radar interferometry. Nature 407:993–996

Cantagrel JM, Gourgaud A, Robin C (1984) Repetitive mixing events and Holocene pyroclastic activity at Pico de Orizaba and Popocatepetl (Mexico). Bull Volcanol 47:735–748

Carrasco-Nunez G (1997) Lava flow growth inferred from morphometric parameters; a case study of Citlaltepetl volcano, Mexico. Geology 134:151–162

Carrasco-Nunez G, Ban M (1994) Geologic map and structure sections of the Citlaltepetl volcano summit area: with summary of the geology of the Citlaltepetl volcano summit area. Cartas geologicas y mineras 9, Instituto de Geologia, UNAM, Mexico

Carrasco-Nunez G, Gomez-Tuena A (1997) Volcanogenic sedimentation around Citlaltepetl (Pico de Orizaba) volcano and surroundings, Veracruz, Mexico. IAVCEI Gen Assem excursions. Mexico DF Universidad Nacional Autonoma Mexico Instituto Geologica Excursion 16:131–151

Carrasco-Nunez G, Rose WI (1995) Eruption of a major Holocene pyroclastic flow at Citlaltepetl volcano (Pico de Orizaba) Mexico, 8.5–9.0 ka. J Volcanol Geotherm Res 69:197–215

Carrasco-Nunez G, Vallance JW, Rose WI (1993) A voluminous avalanche-induced lahar from Citlaltepetl Volcano, Mexico: implications for hazard assessment. J Volcanol Geotherm Res 59:35–46

Costa JE (1984) Physical geomorphology of debris flows. In: Costa JE, Fleisher PJ (eds) Developments and applications of geomorphology. Springer, Berlin Heidelberg New York, pp 268–317

Crandell DR (1971) Postglacial lahars from Mount Rainier Volcano, Washington. US Geol Surv Prof Paper 677

Crandell DR (1989) Gigantic debris avalanche of Pleistocene age from ancestral Mount Shasta volcano, California, and debris-avalanche hazard zonation. US Geol Surv Bull 1861

Day SJ (1996) Hydrothermal pore fluid pressure and the stability of porous, permeable volcanoes. In: McGuire WJ, Jones AP, Neuberg J (eds) Volcano instability on the Earth and other planets. Lond Geol Soc Spec Publ 110:77–93

Firth IR, Watters RJ, Bowman SD (2000) Modeling of volcano edifice and flank stability and implications for hazard zonation. In: Girard J, Liebman M, Breeds C, Doe T (eds) Pacific rocks 2000, Proc Fourth N Am Rock Mech Symp. Balkema, Rotterdam, pp 291–296

Hall ML, Mothes PA (1997) Cotopaxi volcano, Ecuador: mitigation of debris flow impact-daunting task? Int Assoc Volcanol Chem Earth Interior News 1:1–6

Hedenquist JW, Izawa E, Arribas A, White NC (1996) Epithermal gold deposits: styles, characteristics, and exploration. Resour Geol Spec Publ 1

Henley RW, Ellis AJ (1983) Geothermal systems ancient and modern: a geochemical review. Earth Sci Rev 19:1–50

Hoskuldsson A, Robin C (1993) Late Pleistocene to Holocene eruptive activity of Pico de Orizaba, Eastern Mexico. Bull Volcanol 55:571–587

Hubbard BE (2001) Volcanic hazards mapping using aircraft satellite and digital topographic data: Pico de Orizaba (Citlaltépetl) Mexico. PhD Thesis, State University New York, Buffalo

Lopez DL, Williams SN (1993) Catastrophic volcanic collapse: relation to hydrothermal processes. Science 260:1794–1796

Mooser F, Meyer-Abich H, McBirney AR (1958) Catalogue of active volcanoes of the world: part VI. Central America. Napoli Intl Assoc Volcanol

Reid ME, Christian SB, Brien DL (2000) Gravitational stability of three-dimensional stratovolcano edifices. J Geophys Res 105:6043–6056

Reynolds RW, Geist D, Kurz MD (1995) Physical volcanology and structural development of Sierra Negra volcano, Isabela Island, Galapagos archipelago. Geol Soc Am Bull 107:1398–1410

Rye RO (1993) SEG distinguished lecture: the evolution of magmatic fluids in the epithermal environment: the stable isotope perspective. Econ Geol 88:733–753

Siebe C, Abrams M, Sheridan MF (1993) Major Holocene block-and-ash fan at the western slope of ice-capped Pico de Orizaba volcano, Mexico: implications for future hazards. J Volcanol Geotherm Res 59:1–33

Siebert L (1984) Large volcanic debris avalanches: characteristics of source areas, deposits, and associated eruptions. J Volcanol Geotherm Res 22:163–197

Siebert L, Glicken H, Ui T (1987) Volcanic hazards from Bezymianny- and Bandai-type eruptions. Bull Volcanol 49:435–459

Sillitoe RH (1989) Gold deposits in western Pacific island arcs: the magmatic connection. In: Keays RR, Ransay WRH, Groves DI (eds) The geology of gold deposits: the perspective in 1988. Econ Geol Monogr 6:274–291

Sillitoe RH (1994) Erosion and collapse of volcanoes: causes of telescoping in intrusion-centered ore deposits. Geology 22:945–948

Sillitoe RH, Bonham HF Jr (1984) Volcanic landforms and ore deposits. Econ Geol 79:1286–1298

Ui T (1983) Volcanic dry avalanche deposits-Identification and comparison with non-volcanic debris stream deposits. In: Aramaki S, Kushiro I (eds) Arc volcanism. J Volcanol Geotherm Res 18:135–150

Vallance JW (1999) Postglacial lahars and potential hazards in the White Salmon River system on the southwest flank of Mount Adams, Washington. US Geol Surv Bull 2161

van Wyk de Vries B, Kerle N, Petley D (2000) A sector-collapse forming at Casita volcano. Geology 28:167–170

Voight B (2000) Structural stability of andesite volcanoes and lava domes. Phil Trans R Soc Lond 358:1663–1703

Voight B, Elsworth D (1997) Failure of volcano slopes. Geotechnique 47:1–31

Voight B, Glicken H, Janda RJ, Douglass PM (1981) Catastrophic rockslide avalanche of May 18. In: Lipman PW, Mullineaux DR (eds) The 1980 eruptions of Mount St. Helens, Washington. US Geol Surv Prof Pap 1250:347–378

Voight B, Janda RJ, Glicken H, Douglas PM (1983) Nature and mechanism of the Mount St. Helens rockslide avalanche of 18 May 1980. Geotechnique 33:224–273

Watters RJ, Delhaut WD (1995) Effect of argillic alteration on rock mass stability. In: Haneberg WC, Anderson SA (eds) Clay and shale slope instability. Geol Soc Am Rev Eng Geol 10:139–150

Watters RJ, Zimbelman DR, Bowman SD, Crowley JK (2000) Rock mass strength assessment and significance to edifice stability Mount Rainier and Mount Hood, Cascade Range volcanoes. Pure Appl Geophys 157:957–976

Zimbelman DR (1996) Hydrothermal alteration and its influence on volcanic hazards: Mount Rainier, Washington, a case history. PhD Thesis, University of Colorado, Boulder

Zimbelman DR, Rye RO, Breit GN (2003) Origin of sulfate minerals in active andesitic stratovolcanoes. Chem Geol (in press)